

1 *Supplement of*
2 **Atmospheric teleconnection processes linking winter air**
3 **stagnation and haze extremes in China with regional Arctic sea**
4 **ice decline**

5 Yufei Zou¹, Yuhang Wang², Zuowei Xie³, Hailong Wang¹, Philip J. Rasch¹

6 ¹Atmospheric Sciences and Global Change Division, Pacific Northwest National Laboratory,
7 Richland, WA 99354, USA

8 ²School of Earth and Atmospheric Sciences, Georgia Institute of Technology, Atlanta, GA 30332,
9 USA

10 ³International Center for Climate and Environment Sciences, Institute of Atmospheric Physics,
11 Chinese Academy of Sciences, Beijing, 100029, China

12 *Correspondence to:* Yufei Zou (yufei.zou@pnnl.gov) and Yuhang Wang
13 (yuhang.wang@eas.gatech.edu)

14 **Supplement**

15 **Table S1-S5**

16 **Figure S1-S8**

17 **Reference**

18 **Table S1. The 8 CMIP6 models used in this study**

Model	Modeling Center	Institute ID	Experiment ID	Ensemble
Name				Member
CAMS-CSM1-0	Chinese Academy of Meteorological Sciences	CAMS	Historical (Rong, 2019a) +ssp585 (Rong, 2019b)	r1i1p1f1
CESM2	National Center for Atmospheric Research	NCAR	Historical (Danabasoglu et al., 2019) +ssp585 (Danabasoglu, 2019a)	r1i1p1f1
CESM2-WACCM	National Center for Atmospheric Research	NCAR	Historical (Danabasoglu, 2019b) +ssp585 (Danabasoglu, 2019c)	r1i1p1f1
CanESM5	Canadian Centre for Climate Modeling and Analysis	CCCma	Historical (CCCma, 2019a) +ssp585 (CCCma, 2019b)	r1i1p1f1
EC-Earth3	The European Earth consortium	EC-Earth-Consortium	Historical (EC-Earth, 2019a) +ssp585 (EC-Earth, 2019b)	r1i1p1f1
GFDL-CM4	National Oceanic and Atmospheric Administration, Geophysical Fluid Dynamics Laboratory	NOAA-GFDL	Historical (Guo et al., 2018a) +ssp585 (Guo et al., 2018b)	r1i1p1f1
IPSL-CM6A-LR	Institute Pierre-Simon Laplace	IPSL	Historical (Boucher, et al., 2018) +ssp585 (Boucher, et al., 2019)	r1i1p1f1

MIROC6	JAMSTEC, AORI, NIES, and R-CCS	MIROC	Historical (Tatebe and Watanabe, 2018) +ssp585 (Shiogama, et al., 2019)	r1i1p1f1
--------	-----------------------------------	-------	---	----------

20 **Table S2. The statistical properties of the MCA_Z500 and ECP_PPI indices in the**
 21 **WACCM experiments**

	CTRL		SENSall		SENSr1		SENSr2		SENSr3	
Variables	Z500	PPI	Z500	PPI	Z500	PPI	Z500	PPI	Z500	PPI
Mean	0.0	0.0	0.01	-0.06	-0.07	-0.13	0.01	0.03	0.01	-0.02
Std	0.50	0.44	0.54	0.49	0.51	0.43	0.54	0.54	0.53	0.46
Skewness	0.17	-0.13	-0.66	-0.18	-0.13	0.24	0.73	0.56	-0.39	-0.32
Kurtosis	0.07	-0.78	0.27	0.55	-0.04	-0.52	0.48	-0.38	-0.35	-0.31
p-value ^(a)	0.51	0.21	0.01	0.21	1.00	0.39	0.01	0.01	0.13	0.17
p-value ^(b)	—	—	0.90	0.43	0.30	0.04	0.87	0.61	0.95	0.72

22 ^(a): p values of the Shapiro-Wilk normality test;

23 ^(b): p values of the two-sided Student's t-test for the ensemble mean comparison of the two-paired samples from
 24 CTRL and SENS experiments;

25

26 **Table S3. The bootstrap (nboot=5000) estimates (mean \pm standard deviation) of positive
27 extreme probabilities of the MCA_Z500 and ECP_PPI indices in the WACCM experiments**

	CTRL	SENSall	SENSr1	SENSr2	SENSr3
MAC_Z500	5% \pm 0%	4% \pm 4%	4% \pm 2%	9% \pm 3%	6% \pm 3%
ECP_PPI	5% \pm 0%	6% \pm 3%	2% \pm 1%	11% \pm 3%	6% \pm 2%

28
29

30 **Table S4. The bootstrap (nboot=5000) estimates (mean \pm standard deviation) of positive
31 extreme intensities of the MCA_Z500 and ECP_PPI indices in the WACCM experiments**

	CTRL	SENSall	SENSr1	SENSr2	SENSr3
MAC_Z500	1.01 ± 0.10	0.92 ± 0.08	1.00 ± 0.08	1.27 ± 0.08	1.02 ± 0.08
ECP_PPI	0.87 ± 0.06	0.85 ± 0.06	0.86 ± 0.06	1.16 ± 0.06	0.89 ± 0.05

32

33 **Table S5. Changes in ensemble mean values and probabilities of positive extreme values of**
 34 **ECP_PPI in the CMIP6 models**

	Time	NCEP	CAMS-CSM1-0	CESM2	CESM2-WACCM	CanESM5	EC-Earth3	GFDL-CM4	IPSL-CM6A-LR	MIROC6
Mean	P1	-0.38	-0.36	-0.07	0.03	-0.02	-0.27	0.06	0.12	0.12
	P2	0.30	-0.16	0.20	0.36	0.10	-0.21	0.14	0.08	0.02
	P3	-	-0.23	0.11	0.27	0.22	-0.25	0.26	0.30	0.00
P _{extreme}	P1	5%	5%	5%	5%	5%	5%	5%	5%	5%
	P2	19%	11%	11%	10%	7%	5%	6%	7%	2%
	P3	-	13%	13%	6%	12%	2%	13%	11%	4%

35

36

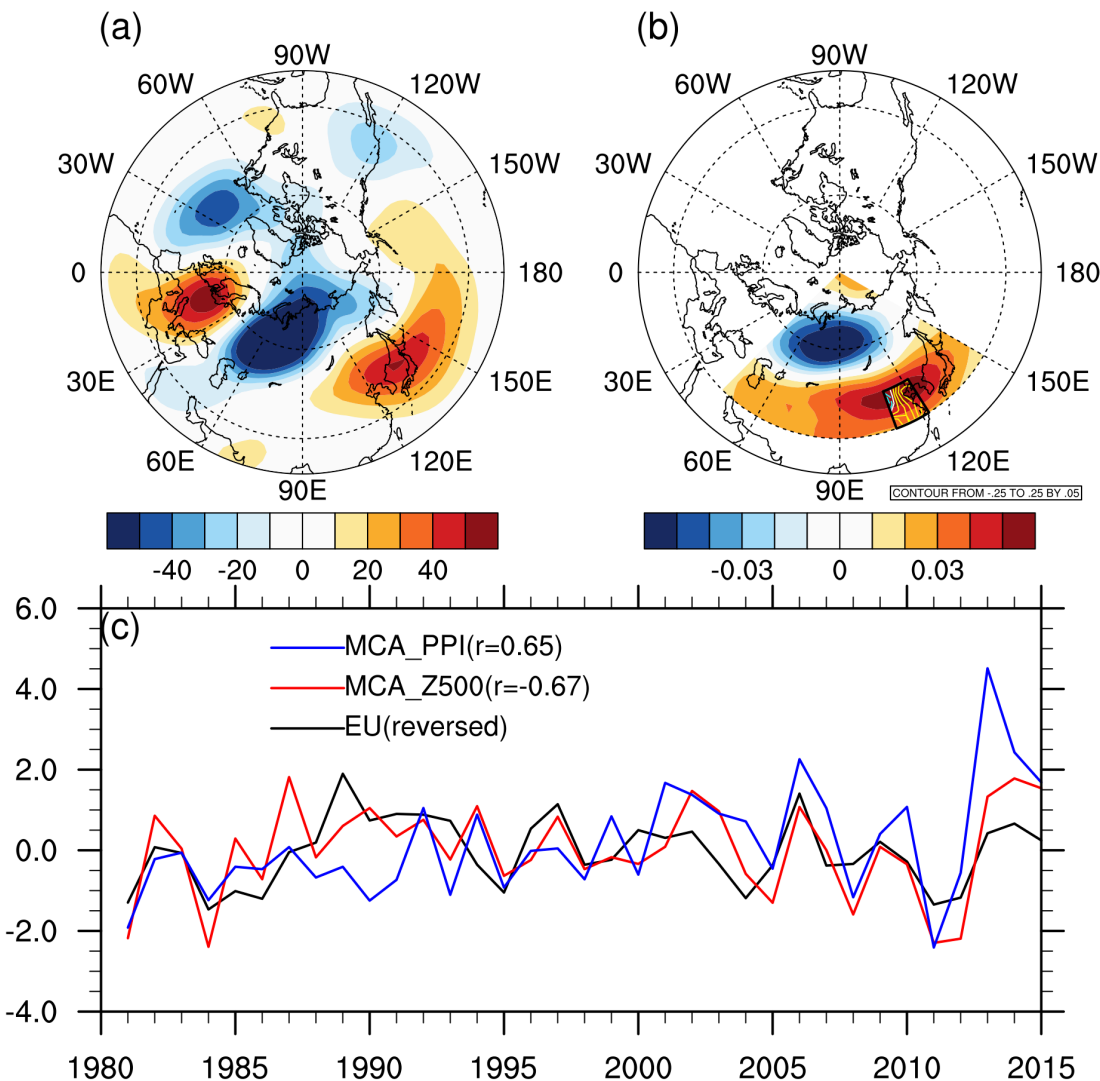
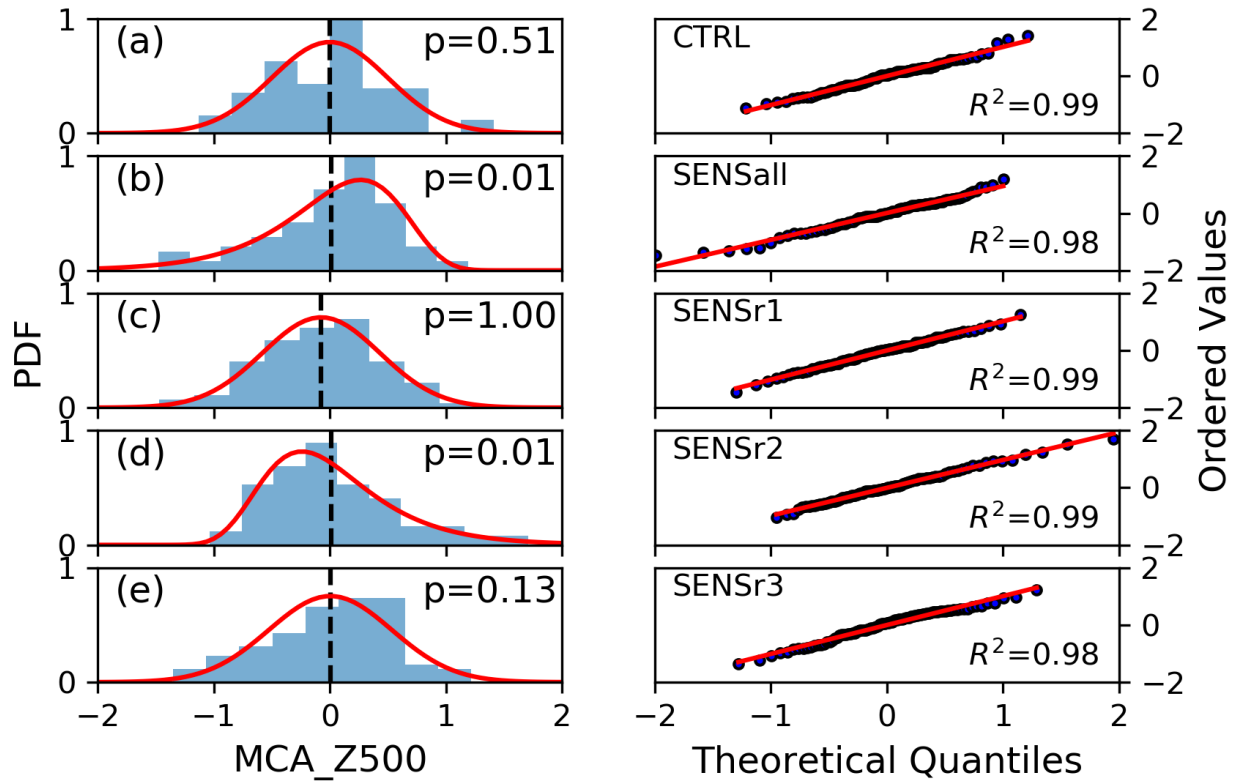
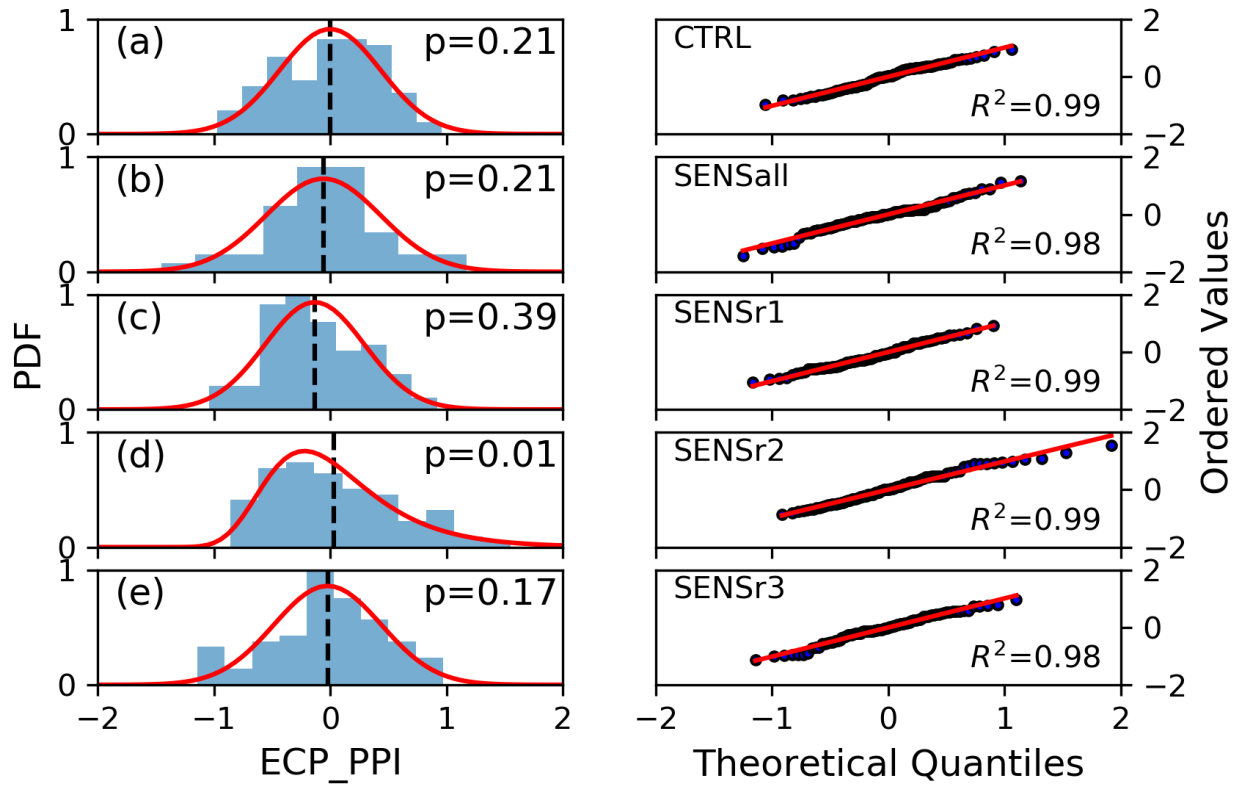


Figure S1. Comparison of the circulation patterns related with regional air stagnation over ECP. (a) spatial distribution of the EU pattern in negative phase (shading) in the 500 hPa geopotential height field (unit: m); (b) spatial distribution of the first modes of MCA_Z500 in positive phase (shading) and MCA_PPI in positive phase (contours with interval of 0.05; the yellow solid lines denote the positive contours; the white line denotes the zero contour; the cyan dashed lines denote the negative contours); the black box denotes the ECP region (112° E to 122° E, 30° N to 41° N); (c) time series of the two circulation patterns and the MCA_PPI index in January from 1981 to 2015. The r value in the parentheses after the MCA_PPI legend is the correlation coefficient between MCA_PPI and MCA_Z500. The r value in the parentheses after the MCA_Z500 legend is the correlation coefficient between MCA_Z500 and EU. The sign of the EU index is reversed for better comparison with the MCA_Z500 index.



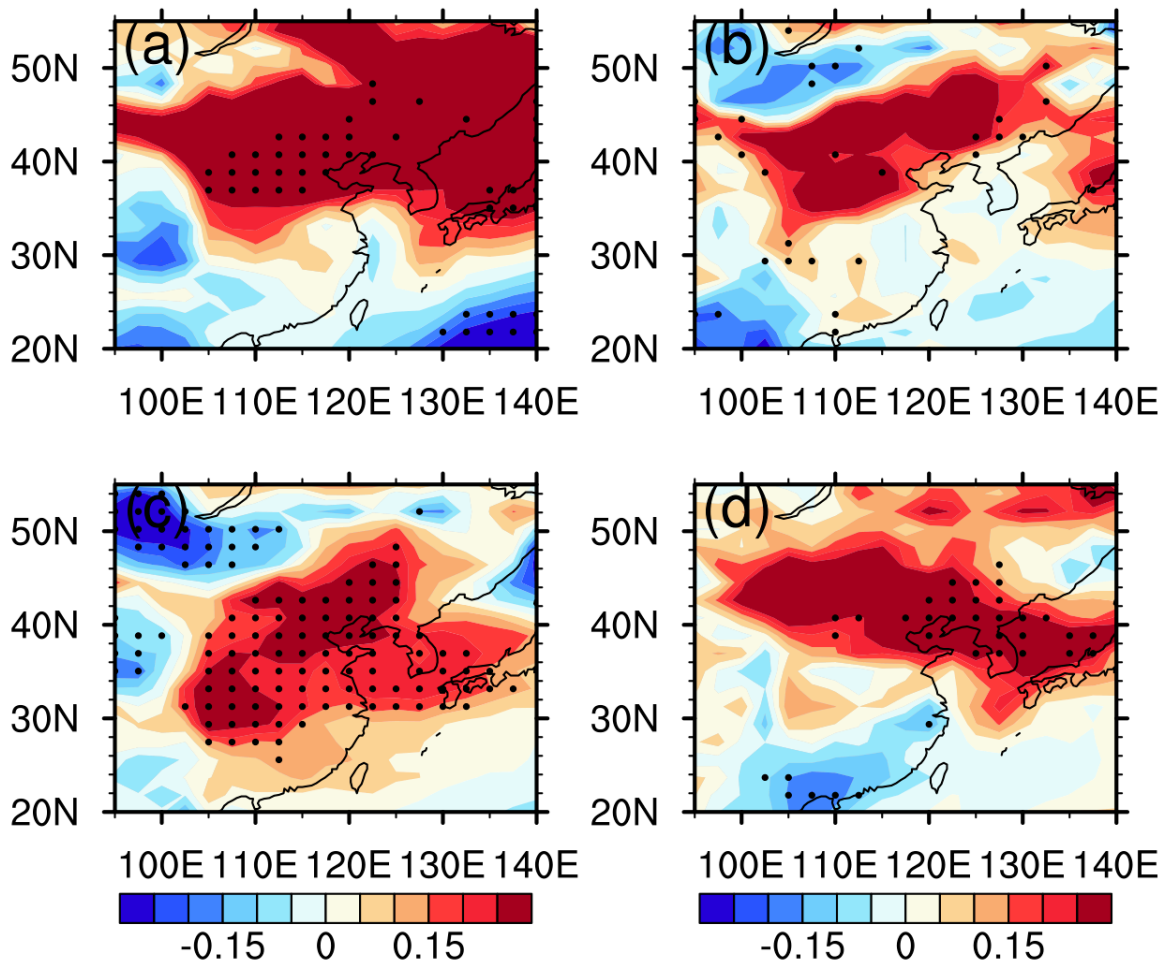
51
52

53 **Figure S2. Evaluation of the MCA_Z500 distribution fitting in the WACCM experiments.**
 54 The left panels show the comparison of the histograms and fitted PDF curves of
 55 MCA_Z500 in winter months (Dec, Jan, and Feb), and the right panels show the Q-Q plots
 56 by comparing the sample quantiles from the corresponding experiments against the
 57 theoretical ones of the distribution. The black dashed lines and p values in the left panel
 58 denote the ensemble means and the normality test results of each experiment, and the red
 59 lines and R^2 values in the right panel denote the least-squares regression fits to the quantile
 60 data and their corresponding goodness-of-fit. The statistical properties in Table S2 and the
 61 histograms of each experiment suggest (a) a normal distribution in CTRL; (b) a left-
 62 skewed distribution with “changed symmetry” in SENSAII; (c) a normal distribution with
 63 “increased variability” in SENSR1; (d) a right-skewed distribution with “changed
 64 symmetry” in SENSR2; (e) a normal distribution with “increased variability” in SENSR3.

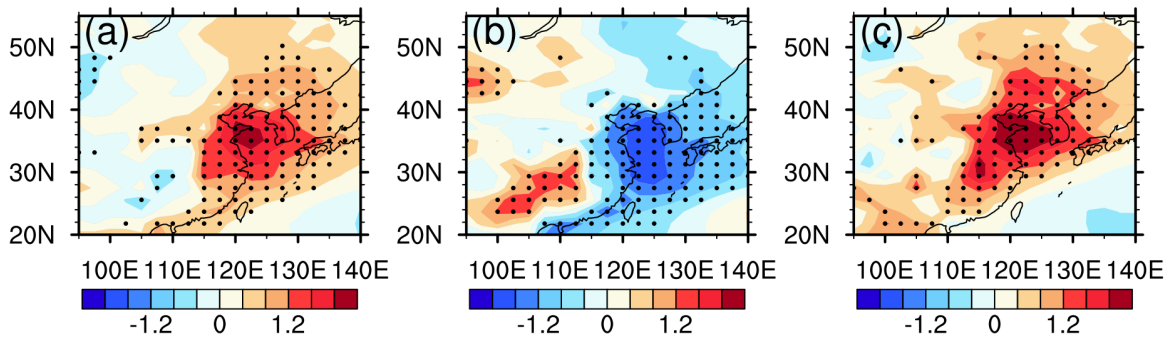


65
66
67
68
69
70
71
72
73
74
75
76
77
78

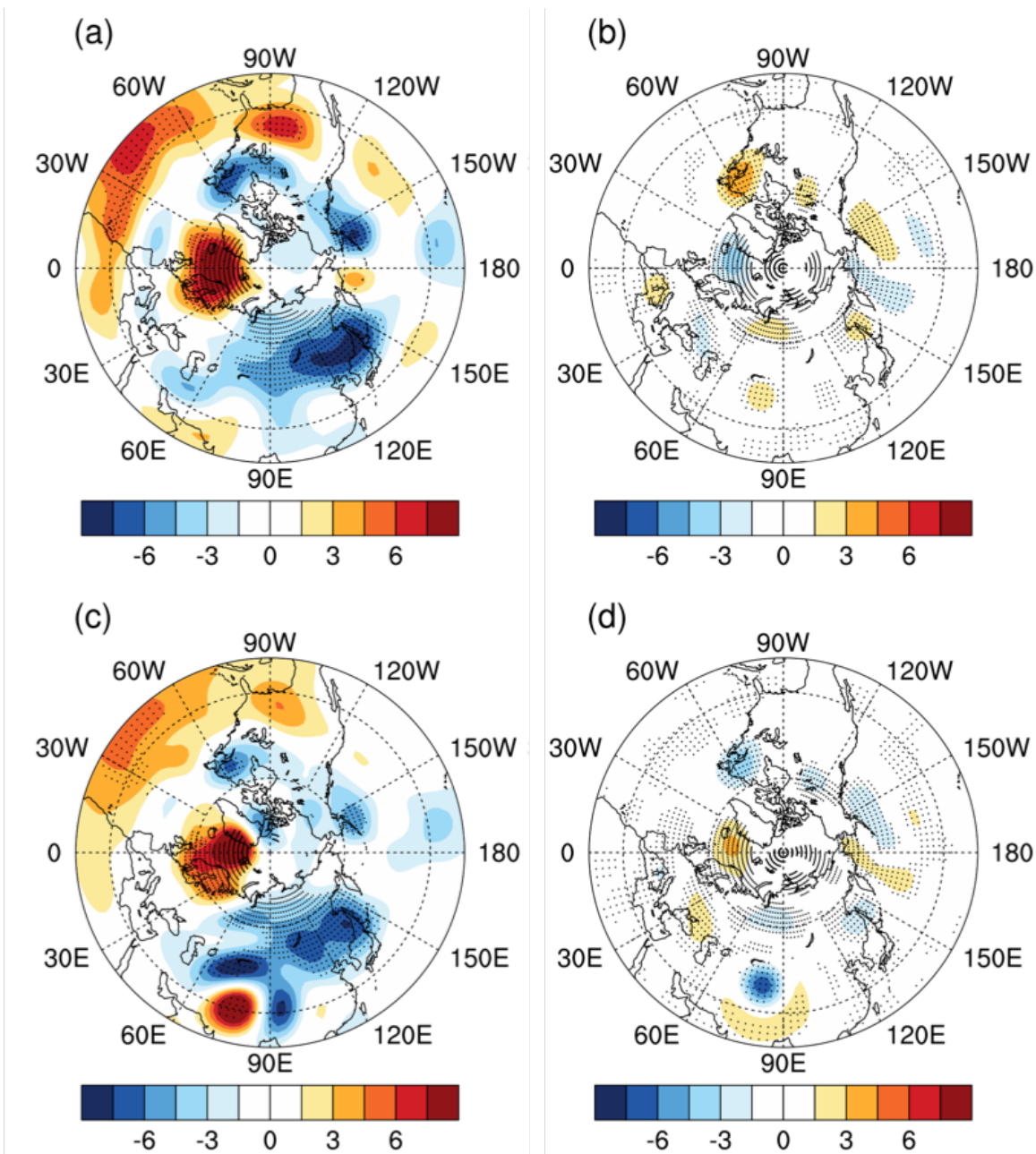
Figure S3. Evaluation of the ECP_PPI distribution fitting in the WACCM experiments.
 The left panels show the comparison of the histograms and fitted PDF curves of ECP_PPI in winter months (Dec, Jan, and Feb), and the right panels show the Q-Q plots by comparing the sample quantiles from the corresponding experiments against the theoretical ones of the distribution. The black dashed lines and p values in the left panel denote the ensemble means and the normality test results of each experiment, and the red lines and R^2 values in the right panel denote the least-squares regression fits to the quantile data and their corresponding goodness-of-fit. The statistical properties in Table S2 and the histograms of each experiment suggest (a) a normal distribution in CTRL; (b) a normal distribution with “increased variability” in SENSAII; (c) a normal distribution with “shifted mean” in SENSR1; (d) a right-skewed distribution with “changed symmetry” in SENSR2; (e) a normal distribution with “increased variability” in SENSR3.



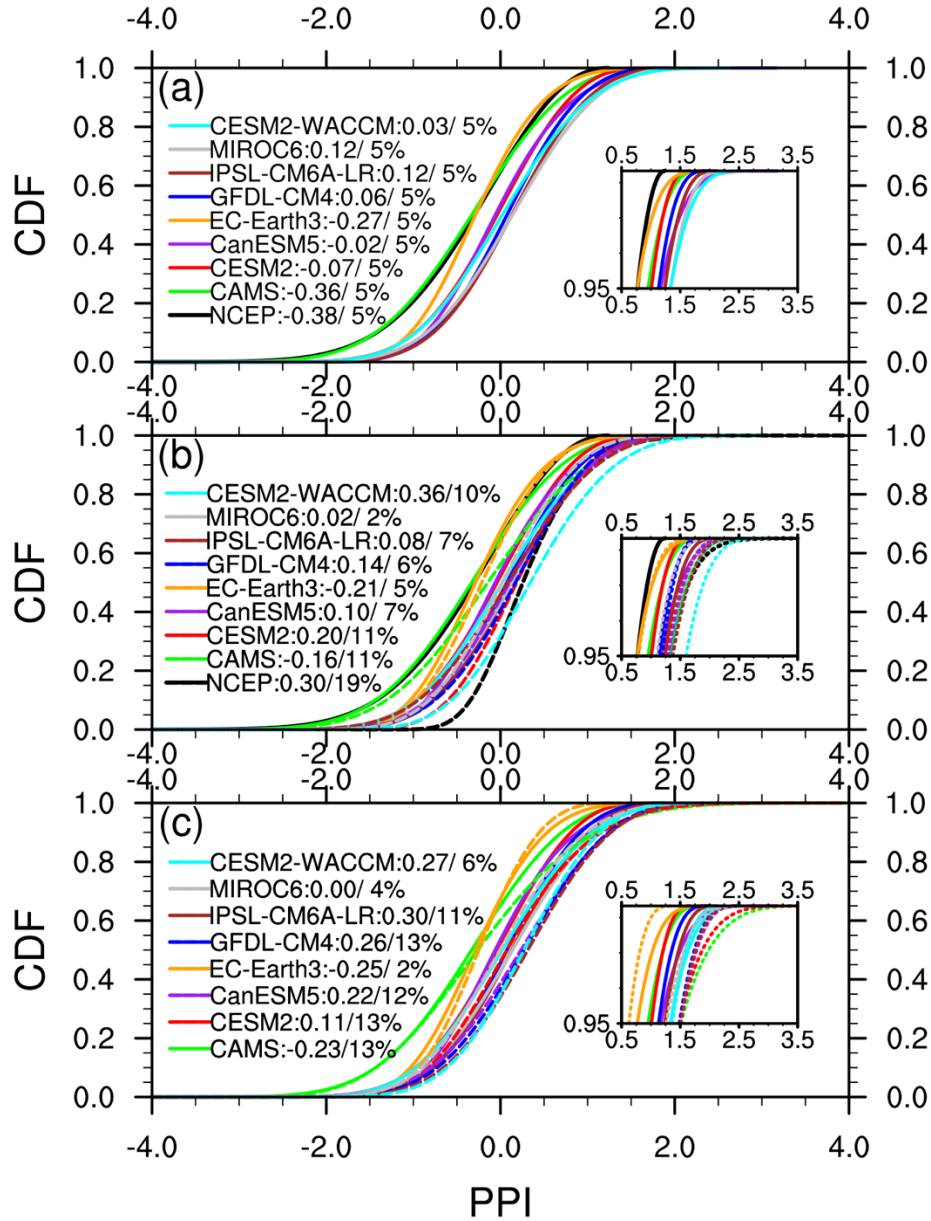
79
80 **Figure S4. Spatial distributions of surface PM_{2.5} concentration relative changes (unit:**
81 **100%) in extreme members of each sensitivity experiment. (a) SENSall; (b) SENSSr1;**
82 **(c) SENSSr2; (d) SENSSr3. The black dots denote the 0.05 significance level.**



83
84
85 **Figure S5. Spatial distributions of regional ventilation condition changes (unitless) in the**
86 **SENSr2 experiment. (a) PPI differences between SENSR2 extreme members and CTRL**
87 **ensemble mean; (b) WSI differences between SENSR2 extreme members and CTRL**
88 **ensemble mean; (c) ATGI differences between SENSR2 extreme members and CTRL**
89 **ensemble mean. The black dots denote the 0.05 significance level.**

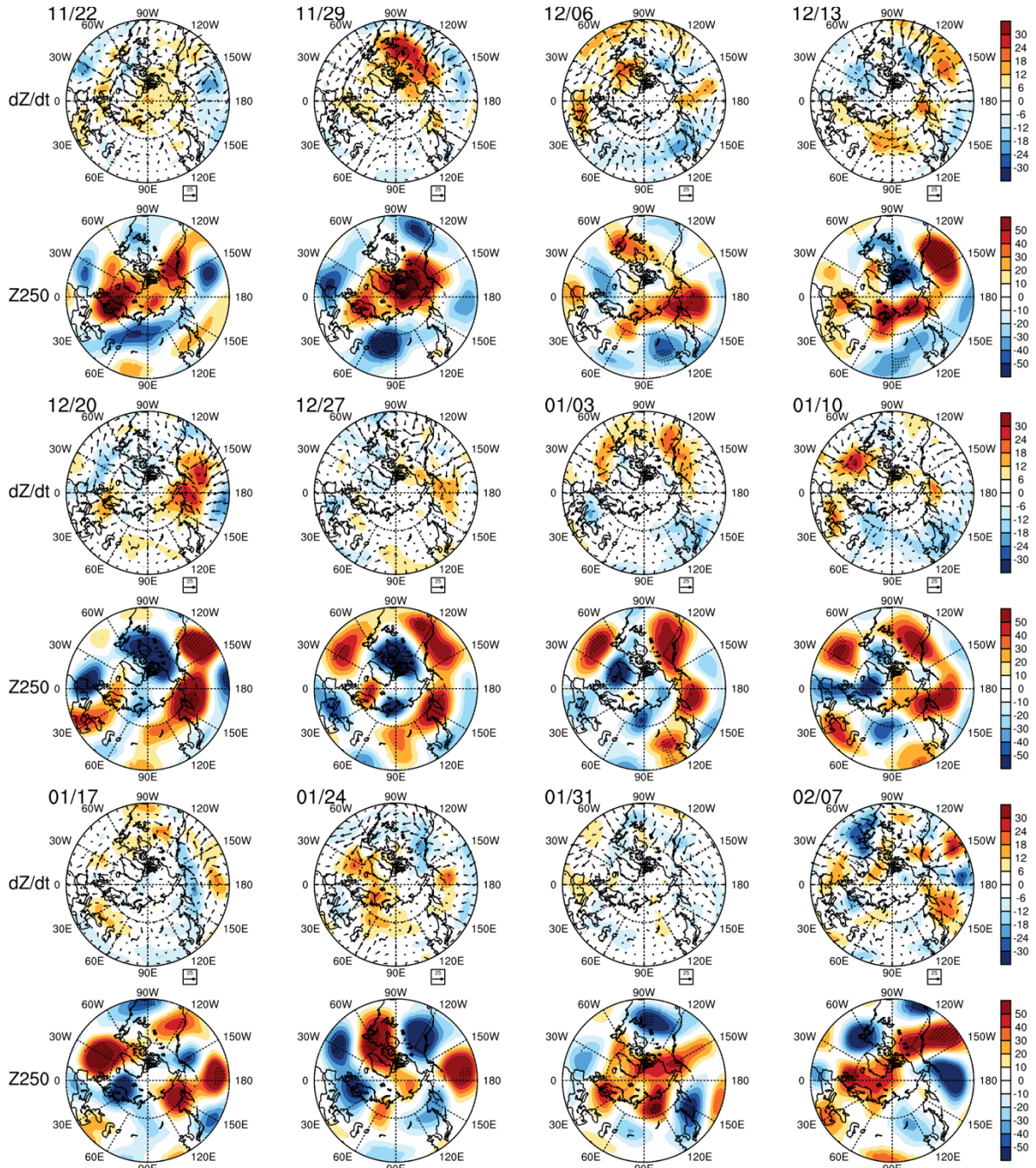


90
91 **Figure S6.** Comparison of geopotential height tendencies (unit: m/day) in the extreme
92 members of WACCM SESN3 driven by (a) transient eddy vorticity forcing (Z_t^V) in the
93 upper troposphere at 250 hPa; (b) transient eddy heat forcing (Z_t^H) at 250 hPa; (c)
94 transient eddy vorticity forcing (Z_t^V) in the lower troposphere at 850 hPa; (d) transient
95 eddy heat forcing (Z_t^H) at 850 hPa. The black dots denote the 0.05 significance level.
96



97
98
99
100
101
102
103
104
105
106

Figure S7. Historical distribution and future projections (under the SSP5-8.5 scenario) of regional air stagnation in winter (DJF) in NCEP reanalysis and CMIP6 models. (a) CDFs of historical ECP_PPI during the P1 period (1951-2000); (b) comparison of ECP_PPI CDFs between historical (solid lines) and near-term projections (dashed lines) during the P2 period (2001-2050). The NCEP ECP_PPI data in P2 are from 2001 to 2019; (c) comparison of ECP_PPI CDFs between historical (solid lines) and long-term projections (dashed lines) during the P3 period (2051-2100). In (a)-(c), the numbers and percentages after each legend name denote ensemble mean values and probabilities of positive extreme values in P1-P3, respectively.



107
108
109
110
111
112

Figure S8. Weekly evolution of E vectors (unit: m^2/s^2), geopotential height tendencies (unit: m/day), and height anomalies (unit: m) at 250 hPa in SENSR2 ensemble mean. The dates on top left corners denote the first days of each week. The black dots in anomalous Z250 fields denote the 0.05 significance level.

- 113 **References**
- 114 Boucher, O., Denvil, S., Caubel, A., et al.: IPSL-CM6A-LR model output prepared for CMIP6
115 CMIP historical. **Version 20180803**. Earth System Grid Federation.
116 <http://doi.org/10.22033/ESGF/CMIP6.5195>, 2018
- 117 Boucher, O., Denvil, S., Caubel, A., et al.: IPSL-CM6A-LR model output prepared for CMIP6
118 ScenarioMIP ssp585. **Version 20190119**. Earth System Grid Federation.
119 <http://doi.org/10.22033/ESGF/CMIP6.5271>, 2019
- 120 CCCma: CCCma CanESM5 model output prepared for CMIP6 CMIP historical. **Version**
121 **20190429**. Earth System Grid Federation. <http://cera->
122 www.dkrz.de/WDCC/meta/CMIP6/CMIP6.CCma.CanESM5.historical, 2018
- 123 CCCma: CCCma CanESM5 model output prepared for CMIP6 ScenarioMIP ssp585. **Version**
124 **20190429**. Earth System Grid Federation. <http://cera->
125 www.dkrz.de/WDCC/meta/CMIP6/CMIP6.ScenarioMIP.CCma.CanESM5.ssp585,
126 2018
- 127 Danabasoglu, G., Lawrence, D., Lindsay, K., et al.: NCAR CESM2 model output prepared for
128 CMIP6 CMIP historical. **Version 20190308**. Earth System Grid Federation.
129 <http://doi.org/10.22033/ESGF/CMIP6.7627>, 2019
- 130 Danabasoglu, Gokhan: NCAR CESM2 model output prepared for CMIP6 ScenarioMIP ssp585.
131 **Version 20190730**. Earth System Grid Federation.
132 <http://doi.org/10.22033/ESGF/CMIP6.7768>, 2019
- 133 Danabasoglu, Gokhan: NCAR CESM2-WACCM model output prepared for CMIP6 CMIP
134 historical. **Version 20190227**. Earth System Grid Federation.
135 <http://doi.org/10.22033/ESGF/CMIP6.10071>, 2019
- 136 Danabasoglu, Gokhan: NCAR CESM2-WACCM model output prepared for CMIP6
137 ScenarioMIP ssp585. **Version 20190815**. Earth System Grid Federation.
138 <http://doi.org/10.22033/ESGF/CMIP6.10115>, 2019
- 139 EC-Earth Consortium (EC-Earth): EC-Earth-Consortium EC-Earth3-Veg model output prepared
140 for CMIP6 CMIP historical. **Version 20190605**. Earth System Grid Federation.
141 <http://doi.org/10.22033/ESGF/CMIP6.4706>, 2019
- 142 EC-Earth Consortium (EC-Earth): EC-Earth-Consortium EC-Earth3-Veg model output prepared
143 for CMIP6 ScenarioMIP ssp585. **Version 20190629**. Earth System Grid Federation.
144 <http://doi.org/10.22033/ESGF/CMIP6.4914>, 2019
- 145 Guo, H., John, J.G., Blanton, C., et al.: NOAA-GFDL GFDL-CM4 model output prepared for
146 CMIP6 CMIP historical. **Version 20180701**. Earth System Grid Federation.
147 <http://doi.org/10.22033/ESGF/CMIP6.8594>, 2018
- 148 Guo, H., John, J.G., Blanton, C., et al.: NOAA-GFDL GFDL-CM4 model output prepared for
149 CMIP6 ScenarioMIP ssp585. **Version 20180701**. Earth System Grid Federation.
150 <http://doi.org/10.22033/ESGF/CMIP6.9268>, 2018
- 151 Rong, X.: CAMS CAMS_CSM1.0 model output prepared for CMIP6 CMIP historical. **Version**
152 **20190708**. Earth System Grid Federation. <http://doi.org/10.22033/ESGF/CMIP6.9754>,
153 2019
- 154 Rong, X.: CAMS CAMS_CSM1.0 model output prepared for CMIP6 ScenarioMIP ssp585.
155 **Version 20190708**. Earth System Grid Federation.
156 <http://doi.org/10.22033/ESGF/CMIP6.11052>, 2019

- 157 Shiogama, H., Abe, M., Tatebe, H., et al.: MIROC MIROC6 model output prepared for CMIP6
158 ScenarioMIP ssp585. **Version 20190627**. Earth System Grid Federation.
159 <http://doi.org/10.22033/ESGF/CMIP6.5771>, 2019
- 160 Tatebe, H. and Watanabe, M.: MIROC MIROC6 model output prepared for CMIP6 CMIP
161 historical. **Version 20181212**. Earth System Grid Federation.
162 <http://doi.org/10.22033/ESGF/CMIP6.5603>, 2018